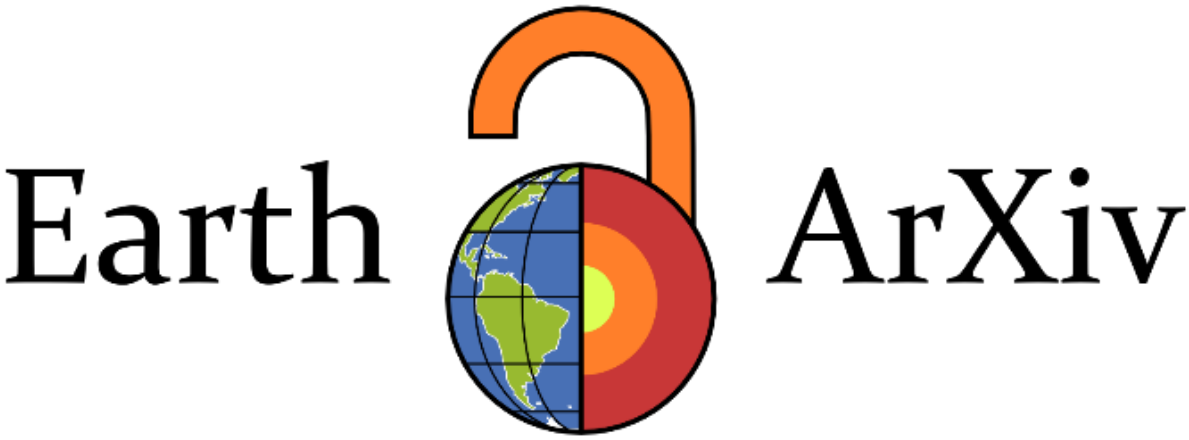

Mineral association drives divergent chemical trajectories of organic sulfur during dryland soil development

Hai-Ruo Mao [a b], Zhuojun Zhang [c], Stephen C. Hart [d e], Jianchao Zhang [f], Mohsen Shakouri [g], and Mengqiang Zhu [h b]*

[a] Institute of Mountain Hazards and Environment, Chinese Academy of Sciences, Chengdu 610213, China

[b] Department of Ecosystem Science and Management, University of Wyoming, Laramie, WY 82071, USA.

[c] State Key Laboratory of Lake and Watershed Science for Water Security, Nanjing Institute of Geography and Limnology, Chinese Academy of Sciences, Nanjing, Jiangsu 211135, China

[d] Department of Life & Environmental Sciences and Sierra Nevada Research Institute, University of California, Merced, CA, 95343, USA

[e] School of Forestry, Northern Arizona University, Flagstaff, AZ, 86011, USA

[f] School of Earth System Science, Institute of Surface-Earth System Science, Tianjin University, Tianjin, 30072, China

[g] Canadian Light Source Inc., University of Saskatchewan, Saskatoon, Saskatchewan, S7N 2V3, Canada

[h] Department of Geological, Environmental, and Planetary Sciences, University of Maryland, College Park, 20742, USA

* Corresponding author: Mengqiang Zhu (mqzhu@umd.edu)

Abstract

Sulfur (S) deficiency is becoming more widespread as atmospheric S deposition declines, increasing ecosystem reliance on mineralization of soil organic S as a source of plant-available sulfate. Yet how organic S chemistry evolves during soil development, and how this evolution is mediated by microbial processing and mineral association, remains poorly understood, particularly in drylands. Here, we used S K-edge X-ray absorption near-edge structure spectroscopy and Fourier transform ion cyclotron resonance mass spectrometry to examine bulk, water-extractable, mineral-associated, and light particulate organic S across a semi-arid soil chronosequence characterized by progressive texture development and increasing microbial activity. Total soil S increased along the chronosequence, with organic S accounting for more than 90% of total S, suggesting that long-term accumulation of atmospherically derived S reflects biological assimilation and stabilization in organic matter, particularly mineral-associated organic matter, rather than passive accumulation of inorganic sulfate alone. Organic S was reorganized into pools with divergent chemical trajectories: water-extractable organic S became less aromatic, more oxidized, and more microbial-derived, reflecting microbial processing and adsorption-induced fractionation; mineral-associated organic S remained enriched in oxidized S species, consistent with retention of oxidized groups by fine minerals; and light particulate organic S became progressively more reduced, consistent with preferential loss of oxidized S from the weakly protected particulate pool. Despite increases in microbial activity and total organic S, the proportion of phosphate-extractable sulfate remained stable, indicating that immediate S availability was buffered rather than simply increasing with microbial processing. These patterns support a mineral-filtering model in which increasing silt- and

clay-sized mineral surfaces during soil development progressively reorganize organic S between weakly protected particulate matter and stabilized mineral-associated organic matter. By stabilizing organic S and retaining released sulfate in an exchangeable, plant-available form, these mineral surfaces buffer sulfate supply.

Keywords: organic sulfur; drylands; mineral-associated organic matter; sulfur speciation; soil chronosequence

1. Introduction

Sulfur (S) is an essential macronutrient for plant growth and a key element in ecosystem functioning (Eriksen, 2009; Bern et al., 2015; Gupta and Germida, 2021). Historically, atmospheric deposition supplied substantial S to many terrestrial ecosystems, but recent emission controls have greatly reduced atmospheric S inputs (Santana et al., 2021; Zhang et al., 2024). As external S inputs decline, microbial mineralization of soil organic S, the dominant form of S in most soils, is expected to become increasingly important for sustaining plant-available sulfate (Eriksen, 2009; Blum et al., 2013; Turner et al., 2016; van Veelen et al., 2020). This transition is especially relevant for drylands, which cover about 45% of Earth's land surface, support more than two billion people, and constitute the largest terrestrial biome (Delgado-Baquerizo et al., 2013; Prăvălie, 2016). In these systems, water limitation constrains both plant inputs and microbial activity, potentially altering the balance between organic S transformation, stabilization, and sulfate release.

The classical framework for soil organic S cycling emphasizes biochemical form. Organic S is commonly divided into ester-bonded S, such as ester sulfate, and carbon-bonded S, such as amino-acid-derived S, organic sulfides, sulfoxides, and sulfonates (McGill and Cole, 1981; Eriksen, 2009). Microbial mineralization can release sulfate through intracellular oxidation of C-bonded S or through extracellular enzymatic hydrolysis of ester-bonded S (McGill and Cole, 1981; Eriksen, 2009). These transformations generally increase the oxidation state of organic S during decomposition (Schroth et al., 2007; Solomon et al., 2011; Prietzel et al., 2013; Tanikawa et al., 2022). However, highly oxidized S compounds may also be rapidly hydrolyzed and lost from organic matter, leaving residual organic S that is not necessarily more oxidized after decomposition (Blum et al., 2013). Thus, biochemical form provides an essential starting point for understanding organic S reactivity, but it does not fully explain why some organic S persists whereas other S is mineralized or lost.

A key unresolved dimension is how organic S chemistry is distributed among soil organic matter fractions that differ in accessibility, protection, and turnover. The particulate organic matter (POM) and mineral-associated organic matter (MAOM) framework provides a useful way to place organic S chemistry within this physical context. In soil carbon research, POM is generally considered a relatively weakly protected pool derived largely from plant residues, whereas MAOM consists of organic compounds associated with silt- and clay-sized minerals and is often more microbially processed and longer-lived (Lavallee et al., 2020; Cotrufo and Lavallee, 2022). Applying this framework to organic S suggests that the same S functional group may have different persistence depending on whether it resides in dissolved organic matter, particulate organic matter, or mineral-

associated organic matter (Fig. 1). A recent continental-scale study showed that mineral-associated organic S (MAOS) accounts for a large fraction of total soil S and is more decomposed, chemically diverse, and climate-sensitive than particulate organic S (POS) (Zhang et al., 2026). What remains unresolved is how such fraction-specific chemical differentiation develops through time during soil formation, especially where texture, microbial activity, and hydrologic conditions change together.

The Substrate Age Gradient of Arizona (SAGA), a 3-million-year semi-arid soil chronosequence in northern Arizona, provides a well-constrained system for examining this question. The sites share similar parent material, climate, and relief, but surface soils become progressively finer textured with increasing substrate age. Silt and clay contents, volumetric soil water content, pore space, microbial biomass, and microbial activity all increase along the chronosequence, whereas soil organic carbon and net primary production peak at intermediate ages before declining at the oldest site, likely due to phosphorus limitation (Selmants and Hart, 2008; Newman and Hart, 2015; Mao et al., 2025). Previous work at SAGA showed that soil organic C chemistry is shaped by coupled microbial processing and mineral retention, with bulk soil organic matter becoming enriched in plant-derived aromatic C and microbial C while water-extractable organic matter becomes depleted in aromatic C and enriched in non-aromatic C during soil development (Mao et al., 2025). These known C trajectories make SAGA an informative setting for testing whether soil organic S follows a similar mineral- and microbially mediated chemical evolution.

Here, we ask whether soil organic S evolves as a single progressively decomposed pool during soil development or instead separates into chemically divergent pools

depending on mineral association. We hypothesized that increasing soil development would lead to three linked outcomes: (1) bulk and water-extractable organic S would become more microbially processed and oxidized; (2) mineral-associated and particulate organic S would diverge in oxidation state if mineral association selectively preserves oxidized S species that are otherwise lost from weakly protected particulate matter; and (3) exchangeable sulfate would not simply track microbial activity or total organic S if mineral stabilization and sulfate adsorption buffer immediate S availability. To test these predictions, we partitioned soil organic S into water-extractable organic S (WEOS), light particulate organic S (LPOS), and mineral-associated organic S (MAOS), characterized bulk, MAOS, and LPOS speciation using S K-edge X-ray absorption near-edge structure (XANES) spectroscopy, and resolved WEOS molecular composition using electrospray ionization Fourier transform ion cyclotron resonance mass spectrometry (ESI FT-ICR-MS).

2. Materials and methods

2.1 Study sites and ecosystem properties

The SAGA chronosequence is located within the San Francisco Volcanic Field in northern Arizona, USA, and includes four sites with substrate ages of 1 ky, 55 ky, 750 ky, and 3000 ky. The sites share similar parent material (microporphyritic basalt cinders), low relief (<1% slope), and present-day climate, with mean annual air temperature of approximately 11 °C and mean annual precipitation of approximately 340 mm. Surface mineral soils (0-15 cm) were collected from under tree canopies, including pinyon pine (*Pinus edulis*) and one-seed juniper (*Juniperus monosperma*), and from inter-canopy spaces, where vegetation shifted from shrubs at the youngest site to grass at the three older

sites (Selmants and Hart, 2008; Newman and Hart, 2015). Four replicate samples were collected and stored air-dry (Mao et al., 2024). Soils are circumneutral, with pH values between 6.0 and 7.1 and no consistent trend with substrate age. Additional site information, including elevation, climate, soil classification, and dust contribution, is provided in Table 1 and in Selmants and Hart (2008).

Soil physical, chemical, and microbial properties changed systematically with substrate age. Silt + clay content increased from 3.0% to 85.1%, and volumetric soil water content increased from 6% to 18% (Mao et al., 2024). Soil organic carbon (SOC) concentration peaked at the 750-ky site before declining at the 3000-ky site, and net primary production followed a similar pattern, apparently because of phosphorus limitation at the oldest substrate (Selmants and Hart, 2008; Newman and Hart, 2015). In contrast, microbial biomass C (MBC) and the MBC/SOC ratio generally increased with substrate age (Table 2). Microbial necromass C relative to SOC also increased substantially with substrate age (Mao et al., 2024).

2.2 Fractionation and quantification of soil sulfur

Exchangeable inorganic sulfate, used here as a proxy for bioavailable S, was extracted with 0.016 mol L^{-1} KH_2PO_4 at a soil-to-solution ratio of 1:20 (Wilhelm Scherer, 2009; Xu et al., 2016; Zhang et al., 2024). Suspensions were centrifuged, and supernatants were filtered before sulfate concentrations were measured by ion chromatography (Thermo ICS 5000). Bulk organic S was operationally estimated as total S minus exchangeable sulfate, because sulfides are not expected to occur in appreciable amounts in these dry, oxic soils (Blum et al., 2013; Kopittke et al., 2016).

MAOM, light POM, and heavy POM fractions were isolated using the size and density fractionation protocol described in Mao et al. (2024), with sodium polytungstate (SPT) solution at a density of 1.85 Mg m^{-3}. Light POM was defined as the density fraction <1.85 Mg m^{-3}. The remaining heavy fraction (>1.85 Mg m^{-3}) was sieved at 53 µm to separate heavy POM (>53 µm) from MAOM (<53 µm). Carbon, nitrogen, and S concentrations of bulk soils, LPOM, and MAOM were determined using an elemental analyzer (Thermo Fisher Isolink EA). The HPOM fraction was not measured because little organic matter was attached to coarse sands, resulting in S concentrations below the detection limit (Leuthold et al., 2022). MAOS and LPOS concentrations on a bulk soil basis were calculated from S concentrations in the isolated fractions and their corresponding mass recoveries.

2.3 Sulfur K-edge XANES spectroscopy

Sulfur K-edge XANES spectroscopy was used to characterize S oxidation-state classes in bulk soils, MAOM, and LPOM at the SXRMB beamline of the Canadian Light Source. Samples were finely ground and mounted as thin films on double-sided carbon tape affixed to copper holders. Two or three fluorescence-mode scans were collected for each sample and averaged. The scan range was 2450-2530 eV, with step sizes of 1.0 eV in the pre-edge region, 0.15 eV across the S K-edge, and 0.75 eV in the post-edge region. Energy was calibrated using $CaSO_4$ with a white-line energy of 2482.8 eV (Manceau and Nagy, 2012).

XANES spectra were normalized using ATHENA (Ravel and Newville, 2005) and fitted in Fityk (Wojdyr, 2010) with six Gaussian functions (G1-G6) and two arctangent

functions following Manceau and Nagy (2012). The Gaussian curves represent exocyclic S (G1), heterocyclic S (G2), sulfoxide (G3), sulfone (G4), sulfonate (G5), and sulfate or ester-sulfate species (G6) (Manceau and Nagy, 2012). Gaussian peak areas were corrected for changes in absorption cross-section with increasing oxidation state using the generic calibration curve:

$$y = 0.3841x - 909.97 \quad (1)$$

where x is the energy of the absorption maximum of a Gaussian curve and y is the scaling factor (Manceau and Nagy, 2012). Relative abundances were calculated as each corrected Gaussian area divided by the sum of all corrected Gaussian areas.

The decomposition index, which reflects changes in soil organic S groups during microbial decomposition of litter (Schroth et al., 2007), was calculated as (Turner et al., 2016):

$$\text{Decomposition index} = (FG5 + FG6)/(FG1 + FG2 + FG3) \quad (2)$$

where FG represents the relative abundance of each S group. Higher values indicate a more decomposed or oxidized organic S pool. The electronic oxidation state (EOS) values of individual S species were calculated as:

$$EOS = 0.6179x - 1529 \quad (3)$$

where x is the white-line peak energy (Zeng et al., 2013; Zhu et al., 2016). The EOS can differ from formal oxidation state, especially for reduced S in complex organic compounds (Xia et al., 1998; Zhu et al., 2016). EOS values were rounded to integers for high-valency S species (EOS > 4) and reported as calculated for low-valency S species (EOS <= 4) (Xia et al., 1998; Zhao et al., 2006; Zhu et al., 2016). Average S oxidation state (ASOX) was calculated as:

$$ASOX = \Sigma(F_{Gi} \times EOS_i) \quad (4)$$

where F_{Gi} is the relative abundance of S group i and EOS_i is the corresponding electronic oxidation state.

2.4 FT-ICR-MS analysis of water-extractable organic sulfur

Water-extractable organic matter was obtained by mixing bulk soil with Milli-Q water at a 1:5 soil-to-water ratio. Suspensions were shaken for 8 h (Li et al., 2018), centrifuged at 2800 g and 4 °C for 20 min, and filtered through 0.22 µm PTFE membranes. Filtrates were desalted and concentrated using PPL cartridges (Bond Elut PPL, 100 mg, 3 mL) following Dittmar et al. (2008) and Li et al. (2018). Briefly, cartridges were rinsed with methanol and acidified water (pH 2), acidified samples were passed through the cartridges, and retained organic matter was eluted with methanol after rinsing and drying with N_2 gas. WEOM extracts were stored at -20 °C before analysis, and procedural blanks were prepared using a water-methanol mixture.

WEOM samples were analyzed using a Bruker Daltonics 12 T Apex-Qe FT-ICR MS at Old Dominion University with electrospray ionization in negative-ion mode. External and internal standards were used for calibration (Chen et al., 2018; Coward et al., 2019). Peaks with signal-to-noise ratios >=5 were exported for molecular formula assignment. Peaks detected in PPL extraction blanks and solvent blanks were removed. Molecular formulas were assigned within the following elemental ranges: $C_{2\text{-}50}$, $H_{2\text{-}100}$, $N_{0\text{-}7}$, $O_{0\text{-}30}$, $S_{0\text{-}3}$, and $P_{0\text{-}2}$. Instrumental parameters and molecular formula assignments have been described in detail (Chen et al., 2018; Coward et al., 2019). Because the present study focuses on organic S, only S-containing molecules were evaluated. Assigned molecules

were classified into eight biochemical classes using van Krevelen space (O/C versus H/C; Table S1): amino sugar, carbohydrate, condensed aromatic, lignin, lipid, protein, tannin, and unsaturated hydrocarbon (Tfaily et al., 2015; Boye et al., 2017).

Molecular indices were calculated for S-containing compounds. Double-bond equivalence (DBE), representing the sum of double bonds and rings in a molecule, was calculated as DBE = 1 + C + 0.5*(N - H + P) (Koch and Dittmar, 2006), where C, H, N, and P are atomic counts in each assigned formula. The modified aromaticity index (AI_{mod}) was calculated as AI_{mod} = (1 + C - 0.5*O - S - 0.5*(N + P + H))/(C - 0.5*O - N - S - P) (Koch and Dittmar, 2016). Intensity-weighted average DBE, AI_{mod}, O/C, and O/S values were calculated following Hawkes et al. (2020).

2.5 Statistical analyses

Differences among substrate ages and canopy types were evaluated separately using one-way analysis of variance, grouping data by the respective factor. Significant differences were identified using Fisher's LSD post hoc test or, when assumptions of normality or homogeneity of variance were not met, the non-parametric Kruskal-Wallis test with post hoc comparisons in the *agricolae* package. Normality and homogeneity of variance were assessed using Shapiro-Wilk and Levene's tests, respectively. Statistical analyses were performed in R 4.1.2. Statistical significance was determined at $P < 0.05$, and different letters indicate significant differences among groups. Relationships between soil properties and S parameters were assessed using Spearman rank correlations and visualized as a heatmap. Because substrate age, silt + clay content, moisture, and microbial

activity covary along the SAGA chronosequence, correlation results were interpreted as associations rather than direct evidence of causation.

3. Results

3.1 Organic S accumulation and redistribution among solid fractions

Soil S accumulated strongly during early to intermediate stages of soil development. Total soil S increased from 0.055-0.097 g kg^{-1} at the 1-ky site to 0.212-0.224 g kg^{-1} at the 750-ky site ($p < 0.05$), followed by a slight, non-significant decline to 0.20-0.21 g kg^{-1} at the 3000-ky site ($p > 0.05$; Fig. 2a; Table S2). Organic S showed the same broad pattern, increasing from approximately 0.05 g kg^{-1} to approximately 0.21 g kg^{-1} across the chronosequence (Fig. 2b). Organic S accounted for 91-96% of total soil S and showed no significant trend in its proportional contribution across substrate age ($p > 0.05$; Fig. 2c). Exchangeable S also increased with substrate age (Fig. 2d), but represented only 3.7-8.7% of total S (Fig. 2e), and its proportion did not vary significantly with substrate age ($p > 0.05$; Fig. 2e).

Partitioning of organic S shifted strongly toward mineral-associated pools during soil development. The S concentration of the isolated MAOM fraction decreased from 0.29-0.35 g kg^{-1} silt + clay at the 1-ky site to 0.17-0.18 g kg^{-1} silt + clay at older sites ($p < 0.05$; Fig. 3a). However, because the mass of the fine fraction increased substantially, MAOS concentration expressed on a bulk-soil basis increased from 0.008-0.025 to 0.15-0.18 g kg^{-1} soil with substrate age ($p < 0.05$; Fig. 3b). Consequently, MAOS increased from 18% of total organic S at the 1-ky site to 85% at the 750-ky site ($p < 0.05$), after which it remained high at the 3000-ky site ($p > 0.05$; Fig. 3c).

LPOM contained substantially higher S concentrations than MAOM, but LPOM S concentration declined with substrate age. The S concentration of the isolated LPOM fraction decreased from 1.6-4.4 g kg^{-1} LPOM at the 1-ky site to approximately 1.6-1.7 g kg^{-1} LPOM at the 750-ky site, with most change occurring between the two youngest sites ($p < 0.05$; Fig. 3d). In contrast, LPOS concentration on a bulk soil basis did not change significantly with substrate age, ranging from 0.02 to 0.06 g kg^{-1} soil ($p > 0.05$; Fig. 3e). The proportion of LPOS in total organic S declined from 43% at the 1-ky site to 16% at the 55-ky site ($p < 0.05$), remained near 25% at the 750-ky site, and declined further to 10% at the 3000-ky site ($p < 0.05$; Fig. 3f). These fraction-level variables did not differ significantly among canopy types when analyzed across all sites or within individual substrate ages ($p > 0.05$; Tables S2 and S3).

Bulk SOM C/S ratios ranged from 62 to 117, with a mean of 85 ± 20 (Fig. S1). Relative to bulk SOM, MAOM had lower and less variable C/S ratios, ranging from 52 to 75, with a mean of 64 ± 6.5. Neither bulk SOM nor MAOM showed a clear trend in C/S ratio across substrate age (Fig. S1). Canopy effects were secondary to the substrate-age trends: total S and exchangeable S were higher under tree canopies than in inter-canopy soils at the 1-ky and 55-ky sites, respectively, but most S pools and fraction-level variables did not differ significantly among canopy types (Tables S2 and S3).

3.2 Mineral-associated and particulate organic S followed opposing oxidation-state trajectories

Organic S speciation differed among bulk soil, MAOS, and LPOS, and the direction of change with soil development depended on fraction. In bulk soil, the relative abundance

290 of sulfonate S (G5) increased with substrate age, whereas exocyclic S (G1), heterocyclic S
291 (G2), and sulfoxide S (G3) decreased significantly ($p < 0.05$; Fig. S2). Other S species
292 showed no consistent age-related trends. In LPOS, exocyclic S (G1) and heterocyclic S
293 (G2) increased with substrate age, whereas sulfone S (G4) and sulfonate S (G5) declined
294 significantly ($p < 0.05$; Fig. S3). In contrast, MAOS showed relatively stable S speciation
295 across the chronosequence, with only sulfoxide S (G3) decreasing consistently with
296 substrate age ($p < 0.05$; Fig. S4).

297 Grouping S species by oxidation state further showed that mineral association was
298 linked to enrichment in oxidized S. Reduced S was defined as the sum of exocyclic S (G1)
299 and heterocyclic S (G2), whereas oxidized S was defined as the sum of sulfone S (G4),
300 sulfonate S (G5), and sulfate or ester-sulfate S (G6) (Turner et al., 2016; Poulin et al., 2017).
301 In bulk soil, oxidized S accounted for 45-68% of total organic S, with an average of 56%.
302 MAOS was consistently more oxidized than LPOS, containing 61-74% oxidized S, with
303 an average of 69%, compared with 44-55% and an average of 50% in LPOS.

304 ASOX and the decomposition index showed similar broad patterns among bulk
305 organic S, MAOS, and LPOS, but the decomposition index showed slightly lower within-
306 site variability (Fig. 4). We therefore used the decomposition index as the primary
307 integrated indicator of organic S processing. Bulk organic S generally became more
308 decomposed with substrate age, although the pattern varied among canopy types (Fig. 4b).
309 In inter-canopy soils, the decomposition index increased from 0.89 at the 1-ky site to 1.58
310 at the 750-ky site before declining to 0.98 at the 3000-ky site. Under pine canopies, it
311 remained near 0.70 from the 1-ky to 750-ky sites, then increased sharply to 1.73 at the

312 3000-ky site. Under juniper canopies, it increased steadily from 0.82 to 1.81 with substrate
313 age ($p < 0.05$).

314 The solid fractions diverged from this bulk pattern. MAOS was substantially more
315 decomposed than LPOS across substrate ages (Fig. 4d,f), but its decomposition index
316 remained statistically stable across the chronosequence ($p = 0.19$ overall; $p > 0.05$ within
317 each canopy type; Fig. 4d). By contrast, the LPOS decomposition index declined with
318 substrate age in inter-canopy soils, from 0.74 to 0.46 ($p < 0.01$), with the sharpest decline
319 at the 3000-ky site (Fig. 4f). Under juniper canopies, the LPOS decomposition index
320 decreased from 0.69 to 0.55 ($p < 0.05$), whereas under pine canopies it remained relatively
321 constant near 0.62 ($p > 0.05$). Despite these within-canopy trends, decomposition indices
322 of bulk organic S, MAOS, and LPOS did not differ significantly among canopy types when
323 pooled across substrate ages or within individual age sites ($p > 0.05$; Tables S2 and S3).

324 **3.3 WEOS recorded dissolved-phase microbial processing**

325 S-containing molecules detected in WEOM by FT-ICR-MS were used to
326 characterize WEOS. The proportion of S-containing molecules relative to all WEOM
327 molecules ranged from 1% to 5% and showed no clear trend with substrate age (Fig. 5).
328 Among WEOS molecules, lipid-like compounds fluctuated across the chronosequence,
329 ranging from 6% to 24% of total S-containing molecules. Protein-like molecules increased
330 significantly from 25% to 66% with substrate age ($p < 0.05$), whereas lignin-like molecules
331 declined from 47% to 13% ($p < 0.05$), despite minor variation among canopy types (Fig.
332 5). Other molecular classes were minor components, each accounting for less than 5% of
333 WEOS. Molecular diversity indices, including richness, Shannon diversity, and Gini-

Simpson diversity, showed no consistent trends with either substrate age or canopy type (Fig. S5).

WEOS molecular indices changed systematically with substrate age. The modified aromaticity index (AI_{mod}) decreased from 0.09 ± 0.03 to 0.04 ± 0.01 (Fig. 6a), and double-bond equivalents decreased from 6.89 ± 1.98 to 3.40 ± 0.46 (Fig. 6b). In contrast, O/C and O/S ratios increased from 0.34 ± 0.02 to 0.38 ± 0.03 and from 5.85 ± 0.55 to 7.23 ± 0.14, respectively (Fig. 6c,d). Together, these trends indicate that WEOS molecules became less aromatic, more saturated, and more oxidized during soil development.

3.4 Exchangeable sulfate was decoupled from microbial processing and organic S accumulation

Exchangeable S increased with substrate age in concentration but not as a proportion of total S (Fig. 2d,e). Thus, although total organic S, microbial biomass, and microbial activity increased along the chronosequence, the fraction of soil S present as exchangeable sulfate remained relatively stable. This pattern indicates that stronger microbial processing and larger organic S pools did not translate directly into a greater proportional pool of immediately exchangeable sulfate.

Correlations among S properties and ecosystem variables provide additional context for this decoupling (Fig. 7). The proportion of MAOS in total organic S was positively correlated with silt + clay content, whereas the LPOS decomposition index was negatively correlated with silt + clay content ($p < 0.05$). WEOS molecular composition was also associated with microbial properties: O/C and O/S ratios were positively correlated with MBC/SOC, whereas AI_{mod} and DBE were negatively correlated with

MBC/SOC ($p < 0.05$). Exchangeable S was positively correlated with total organic S but negatively correlated with the LPOS decomposition index ($p < 0.05$). Because silt + clay content covaries with substrate age, soil moisture, and microbial activity along the chronosequence, these relationships are interpreted as associations consistent with mineral filtering rather than as isolated effects of texture alone.

4. Discussion

4.1 Biological assimilation and mineral association retain external sulfur inputs during soil development

The dominance of organic S in total soil S indicates that S accumulation along SAGA reflects biological cycling rather than passive retention of inorganic sulfate alone. Aeolian dust is an important external input to Colorado Plateau soils, supplying fine particles and nutrients to otherwise nutrient-poor semi-arid landscapes (Reynolds et al., 2001; Reynolds et al., 2006). Atmospheric S deposition in the Southern Colorado Plateau is relatively low but measurable, providing a continuing external S source (Sullivan et al., 2011), and atmospherically deposited S occurs primarily as inorganic sulfate (Takahashi et al., 2006). The fact that more than 90% of total S occurred in organic forms therefore implies assimilation of sulfate into biological and organic matter pools, followed by stabilization during soil development. The progressive increase in MAOS from 18% to 85% of organic S is consistent with this interpretation, although it reflects the combined effects of substrate age, texture, moisture, microbial activity, and ecosystem development.

The decline in total S at the oldest site parallels previously reported declines in SOC and net primary production, which have been attributed to phosphorus limitation during

ecosystem retrogression (Selmants and Hart, 2008; Newman and Hart, 2015). This pattern suggests that biological inputs remain important for sustaining S stocks even when mineral surfaces are abundant.

Canopy-associated enrichment of soil S pools at younger sites further indicates that vegetation can influence local S inputs through throughfall, stemflow, dust interception, and litter inputs (Lindberg and Garten, 1988), consistent with fertility-island patterns in drylands (Schlesinger et al., 1996; Coble and Hart, 2013). Specifically, total S was higher under canopies at the 1-ky site, whereas exchangeable S was higher under canopies at the 55-ky site. However, canopy effects weakened at older sites, suggesting that geochemical development and fine-fraction accumulation increasingly dominate over microsite-scale vegetation effects.

4.2 Mineral association preserves oxidized S while particulate organic S loses oxidized groups

A central result of this study is that organic S speciation did not change uniformly during dryland soil development. Although bulk organic S became more decomposed overall, the two solid SOM fractions followed opposing chemical trajectories: MAOS remained persistently oxidized and highly decomposed, whereas LPOS became progressively more reduced. This divergence indicates that bulk organic S patterns can mask contrasting transformations among fractions and that the fate of organic S depends strongly on its association with particulate versus mineral-associated organic matter.

The opposing oxidation-state trajectories of MAOS and LPOS suggest a mineral-filtering mechanism. In the weakly protected particulate pool, reduced S can be oxidized

during microbial decomposition to sulfonate or sulfate/ester-sulfate species. However, because LPOS lacks strong mineral association, these oxidized species may be rapidly hydrolyzed by extracellular enzymes or mineralized to inorganic sulfate (Blum et al., 2013; Zhang et al., 2026), leaving the residual particulate pool enriched in reduced S. This mechanism is consistent with the decline in LPOS decomposition index and with the decreasing S concentration of LPOM with substrate age. It also explains why the LPOS pattern differs from the increase in organic S decomposition index observed during litter decomposition by Schroth et al. (2007): in soils, oxidized S products may not accumulate in the particulate residue if they are rapidly hydrolyzed and lost.

In contrast, MAOS maintained a high decomposition state and oxidized S composition across the chronosequence. MAOS contained a large proportion of oxidized S, including sulfonate and sulfate/ester-sulfate species, and its decomposition index did not decline with substrate age despite increasing microbial activity (Fig. 4d). This persistence is consistent with preferential stabilization of oxidized S compounds in association with silt- and clay-sized minerals (Tanikawa et al., 2022). Ester-sulfate groups can interact strongly with mineral surfaces, and previous studies have reported greater oxidation of organic S in fine or mineral-associated fractions than in bulk or coarse fractions (Prietzel et al., 2007; Tanikawa et al., 2022). Microbial residues may also contribute to the oxidized S composition of MAOS, particularly because microbial biomass and fungal residues can contain substantial S and microbial necromass increases along SAGA (Gupta and Germida, 2021; Heinze et al., 2021; Mao et al., 2024; Zhang et al., 2026).

The persistence of approximately 30% reduced S in MAOS indicates that mineral association does not exclusively stabilize oxidized compounds. Reduced S may enter

MAOM through plant litter that has undergone microbial modification, microbial biomass and necromass, or aggregation of reduced organic matter with fine minerals (Solomon et al., 2001; Turner et al., 2016; Liang et al., 2017; Lavallee et al., 2020; Gupta and Germida, 2021). Thus, the mineral filter is not absolute. Rather, our results suggest that mineral association changes the relative fate of S functional groups: oxidized S compounds that are rapidly lost from weakly protected particulate matter can persist when associated with fine minerals, while reduced S compounds can also be stabilized when incorporated into mineral-associated organic matter.

4.3 WEOS reflects microbial processing and adsorption-induced fractionation

WEOS provided molecular-scale evidence that microbial processing intensified during soil development. The decline in AI_{mod} and DBE indicates decreasing aromaticity and unsaturation, and the increases in O/C and O/S indicate greater oxidation of S-containing dissolved organic molecules (Roth et al., 2013). These trends parallel the broader WEOM patterns reported for SAGA (Mao et al., 2025). They likely reflect both microbial transformation of plant-derived dissolved organic matter and mineral adsorption-induced fractionation during passage through soil. Microbial-derived organic matter, including necromass and metabolites, generally has lower aromaticity and unsaturation than plant-derived organic matter (Fellman et al., 2008; Li et al., 2018; Roth et al., 2019), whereas minerals preferentially retain aromatic compounds from solution (Ding et al., 2020; Hu et al., 2024; Mao et al., 2025).

The molecular-class distribution of WEOS further supports this interpretation. The decline in lignin-like compounds and increase in protein-like compounds indicate a shift

445 from plant-derived aromatic inputs toward microbial-derived or microbially processed
446 molecules. These dissolved S-containing molecules likely form a transfer pool linking
447 plant inputs, microbial biomass, mineral surfaces, and exchangeable sulfate. The positive
448 correlations of the intensity-weighted O/C and O/S ratios of S-containing WEOS molecular
449 formulas with MBC/SOC, together with the negative correlations of their AI_{mod} and DBE
450 values with MBC/SOC (Fig. 7), indicate that greater microbial biomass relative to SOC
451 was associated with less aromatic, more saturated, and more oxidized WEOS molecules.
452 Thus, WEOS is not merely a small soluble pool; it records both microbial transformation
453 and adsorption-induced fractionation during soil development.

454 **4.4 Sulfate availability is buffered by organic S mineralization and mineral retention**

455 Exchangeable sulfate was decoupled from both microbial activity and organic S
456 accumulation. Although microbial biomass, microbial activity, and total organic S
457 increased with substrate age, exchangeable sulfate remained a small and proportionally
458 stable fraction of total S. This pattern indicates that enhanced microbial processing does
459 not necessarily lead to a larger immediate pool of plant-available sulfate. Instead, sulfate
460 availability appears to be buffered by the balance between organic S mineralization and
461 mineral retention.

462 Minerals likely exert this buffering through two linked processes. First, mineral
463 association promotes MAOS formation and protects organic S from rapid enzymatic
464 mineralization, slowing sulfate release. Second, the same fine mineral fractions can adsorb
465 sulfate with moderate binding strength, reducing leaching while maintaining an
466 exchangeable pool that remains potentially available for biological uptake (Eriksen and

Askegaard, 2000; Zhang et al., 2026). The positive correlation between exchangeable S and total organic S suggests that organic S mineralization contributes to sulfate supply, whereas the negative correlation between exchangeable S and the LPOS decomposition index is consistent with rapid loss of oxidized S groups from the labile particulate pool. Together, these patterns suggest that fine minerals can function as both stabilizers of organic S and retainers of mineralized sulfate (Fig. 1).

This dual role has implications for interpreting S availability in developed dryland soils. Microbial activity alone may be a poor predictor of exchangeable sulfate because the products of decomposition can be retained, adsorbed, or incorporated into mineral-associated pools. Similarly, bulk organic S concentration may not indicate immediate S supply if much of the pool is mineral-associated. The size and chemistry of weakly protected particulate organic S, together with the capacity of fine minerals to retain released sulfate, may provide a more mechanistic basis for predicting sulfate availability than bulk organic S or microbial biomass alone.

5. Conclusions

Across this semi-arid soil chronosequence, organic sulfur did not follow a single, progressive decomposition trajectory during soil development. Instead, it partitioned into chemically distinct pools whose trajectories depended on mineral association. As soils became finer textured and more microbially active with substrate age, bulk organic S became more decomposed, and water-extractable organic S shifted toward less aromatic, more oxidized, and more microbial-derived molecules. In contrast, the two solid organic matter fractions diverged: mineral-associated organic S remained consistently oxidized and

highly decomposed, whereas light particulate organic S became progressively more reduced. This opposing behavior is the clearest signal in our data and suggests that soil development partitions organic S not only by physical fraction, but also by oxidation state.

The divergent behavior of MAOS and LPOS points to a mineral-filtering mechanism. In weakly protected particulate organic matter, oxidized S species, particularly sulfate/ester-sulfate species, may be rapidly hydrolyzed or mineralized and lost as inorganic sulfate, leaving the residual LPOS enriched in reduced S. In contrast, comparable oxidized S species persist in MAOS, consistent with stabilization by silt- and clay-sized minerals through adsorption, aggregation, or association with microbial residues. Thus, mineral association appears to alter the chemical fate of organic S, preferentially preserving oxidized S compounds that would otherwise be rapidly transformed or lost from particulate organic matter.

This fraction-specific sorting also helps explain why microbial activity did not translate directly into greater immediate sulfate availability. Although microbial biomass, microbial activity, and total organic S increased along the chronosequence, the proportion of exchangeable sulfate remained relatively stable. Fine mineral fractions may therefore simultaneously promote microbial transformation, stabilize organic S within MAOM, and retain released sulfate on exchange sites. As a result, microbial activity or bulk organic S alone is an incomplete predictor of sulfate supply; the distribution of organic S between particulate and mineral-associated pools, and the chemical state of those pools, may provide a more mechanistic indicator of S availability.

These interpretations remain hypotheses based on fraction-level chemistry and associations along a chronosequence. Because silt and clay content covary with substrate

age, soil moisture, microbial activity, plant inputs, and ecosystem development, this study cannot isolate texture as a single causal driver. Establishing causality will require process-level experiments, including fraction-specific mineralization assays, sulfatase and arylsulfatase measurements, isotope-labeling experiments, and sorption studies that resolve which organic S moieties are preferentially retained by mineral surfaces.

Overall, this study complements the continental-scale POM-MAOM framework for organic sulfur proposed by Zhang et al. (2026) by providing a soil-development perspective on how mineral-associated and particulate S pools become chemically distinct. As atmospheric S deposition declines and ecosystems rely increasingly on organic S mineralization to sustain sulfate supply, distinguishing weakly protected particulate S from stabilized mineral-associated S will be essential for predicting S availability in drylands and other mineral-rich soils. The central implication is that fine minerals do not merely protect organic S; they partition its oxidation state, persistence, and availability during soil development.

Acknowledgements

The authors thank Paul C. Selmants for collecting the soil samples. This work was supported by a U.S. National Science Foundation (NSF) Faculty Early Career Development Program to M.Z. (EAR-1752903). Partial support was from the USDA-NIFA Hatch Multistate (Accession 1021293) and NSF Established Program to Stimulate Competitive Research (EPSCoR) Track 1 RII grant (EPS-1655726) at the University of Wyoming. The SAGA was established by P.C.S. and S.C.H. with the support of an EPA STAR Graduate Fellowship (U-916251), a Merriam-Powell Center for Environmental

Research Graduate Fellowship, an Achievement Rewards for College Scientists (ARCS) Foundation of Arizona Scholarship, and McIntire-Stennis appropriations to Northern Arizona University and the State of Arizona. The S K-edge XANES data were collected at the Canadian Light Source, supported by the Natural Sciences and Engineering Research Council of Canada, the National Research Council Canada, the Canadian Institutes of Health Research, the Province of Saskatchewan, Western Economic Diversification Canada, and operated by the University of Saskatchewan.

Competing Interest Statement

The authors declare that they have no conflict of interest.

Declaration of generative AI use

ChatGPT was used to polish the writing of the manuscript during the manuscript preparation process upon submission of the paper.

Data availability

All data are available in the main text or the supplementary materials.

References

Bern, C.R., Chadwick, O.A., Kendall, C., Pribil, M.J., 2015. Steep spatial gradients of volcanic and marine sulfur in Hawaiian rainfall and ecosystems. Science of the Total Environment 514, 250–260. doi: https://doi.org/10.1016/j.scitotenv.2015.02.001.

Blum, C.S., Lehmann, J., Solomon, D., Caires, E.F., Alleoni, L.R.F., 2013. Sulfur forms in organic substrates affecting S mineralization in soil. Geoderma 200-201, 156–164. doi: https://doi.org/10.1016/j.geoderma.2013.02.003.

Boye, K., Noël, V., Tfaily, M.M., Bone, S.E., Williams, K.H., Bargar, John R., Fendorf, S., 2017. Thermodynamically controlled preservation of organic carbon in floodplains. Nature Geoscience 10, 415. doi: 10.1038/ngeo2940.

Chen, H., Yang, Z., Chu, R.K., Tolic, N., Liang, L., Graham, D.E., Wullschleger, S.D., Gu, B., 2018. Molecular Insights into Arctic Soil Organic Matter Degradation under Warming. Environmental Science & Technology 52, 4555–4564. doi: 10.1021/acs.est.7b05469.

Coble, A.A., Hart, S.C., 2013. The significance of atmospheric nutrient inputs and canopy interception of precipitation during ecosystem development in piñon–juniper woodlands of the southwestern USA. Journal of Arid Environments 98, 79–87. doi: https://doi.org/10.1016/j.jaridenv.2013.08.002.

Cotrufo, M.F., Lavallee, J.M., 2022. Soil organic matter formation, persistence, and functioning: A synthesis of current understanding to inform its conservation and regeneration. Advances in Agronomy 172, 1–66. doi: https://doi.org/10.1016/bs.agron.2021.11.002.

Coward, E.K., Ohno, T., Sparks, D.L., 2019. Direct Evidence for Temporal Molecular Fractionation of Dissolved Organic Matter at the Iron Oxyhydroxide Interface. Environmental Science & Technology 53, 642–650. doi: 10.1021/acs.est.8b04687.

Delgado-Baquerizo, M., Maestre, F.T., Gallardo, A., Bowker, M.A., Wallenstein, M.D., Quero, J.L., Ochoa, V., Gozalo, B., García-Gómez, M., Soliveres, S., García-Palacios, P., Berdugo, M., Valencia, E., Escolar, C., Arredondo, T., Barraza-Zepeda, C., Bran, D., Carreira, J.A., Chaieb, M., Conceição, A.A., Derak, M., Eldridge, D.J., Escudero, A., Espinosa, C.I., Gaitán, J., Gatica, M.G., Gómez-González, S., Guzman, E., Gutiérrez, J.R., Florentino, A., Hepper, E., Hernández, R.M., Huber-Sannwald, E., Jankju, M., Liu, J., Mau, R.L., Miriti, M., Monerris, J., Naseri, K., Noumi, Z., Polo, V., Prina, A., Pucheta, E., Ramírez, E., Ramírez-Collantes, D.A., Romão, R., Tighe, M., Torres, D., Torres-Díaz, C., Ungar, E.D., Val, J., Wamiti, W., Wang, D., Zaady, E., 2013. Decoupling of soil nutrient cycles as a function of aridity in global drylands. Nature 502, 672–676. doi: 10.1038/nature12670.

Ding, Y., Shi, Z., Ye, Q., Liang, Y., Liu, M., Dang, Z., Wang, Y., Liu, C., 2020. Chemodiversity of soil dissolved organic matter. Environmental Science & Technology 54, 6174–6184. doi: 10.1021/acs.est.0c01136.

Dittmar, T., Koch, B., Hertkorn, N., Kattner, G., 2008. A simple and efficient method for the solid-phase extraction of dissolved organic matter (SPE-DOM) from seawater. Limnology and Oceanography: Methods 6, 230–235. doi: 10.4319/lom.2008.6.230.

Eriksen, J., 2009. Chapter 2 Soil Sulfur Cycling in Temperate Agricultural Systems, Advances in Agronomy. Academic Press, pp. 55–89. doi: https://doi.org/10.1016/S0065-2113(09)01002-5.

Eriksen, J., Askegaard, M., 2000. Sulphate leaching in an organic crop rotation on sandy soil in Denmark. Agriculture, Ecosystems & Environment 78, 107–114. doi: https://doi.org/10.1016/S0167-8809(99)00117-6.

Fellman, J.B., D'Amore, D.V., Hood, E., Boone, R.D., 2008. Fluorescence characteristics and biodegradability of dissolved organic matter in forest and wetland soils from coastal

temperate watersheds in southeast Alaska. Biogeochemistry 88, 169–184. doi: 10.1007/s10533-008-9203-x.
Gu, C., Hart, S.C., Turner, B.L., Hu, Y., Meng, Y., Zhu, M., 2019. Aeolian dust deposition and the perturbation of phosphorus transformations during long-term ecosystem development in a cool, semi-arid environment. Geochimica et Cosmochimica Acta 246, 498–514. doi: https://doi.org/10.1016/j.gca.2018.12.017.
Gupta, V.V.S.R., Germida, J.J., 2021. 18 - Microbial transformations of sulfur in soil, In: Gentry, T.J., Fuhrmann, J.J., Zuberer, D.A. (Eds.), Principles and Applications of Soil Microbiology (Third Edition). Elsevier, pp. 489–522. doi: https://doi.org/10.1016/B978-0-12-820202-9.00018-6.
Hawkes, J.A., D'Andrilli, J., Agar, J.N., Barrow, M.P., Berg, S.M., Catalán, N., Chen, H., Chu, R.K., Cole, R.B., Dittmar, T., Gavard, R., Gleixner, G., Hatcher, P.G., He, C., Hess, N.J., Hutchins, R.H.S., Ijaz, A., Jones, H.E., Kew, W., Khaksari, M., Palacio Lozano, D.C., Lv, J., Mazzoleni, L.R., Noriega-Ortega, B.E., Osterholz, H., Radoman, N., Remucal, C.K., Schmitt, N.D., Schum, S.K., Shi, Q., Simon, C., Singer, G., Sleighter, R.L., Stubbins, A., Thomas, M.J., Tolic, N., Zhang, S., Zito, P., Podgorski, D.C., 2020. An international laboratory comparison of dissolved organic matter composition by high resolution mass spectrometry: Are we getting the same answer? Limnology and Oceanography: Methods 18, 235–258. doi: 10.1002/lom3.10364.
Heinze, S., Hemkemeyer, M., Schwalb, S.A., Khan, K.S., Joergensen, R.G., Wichern, F., 2021. Microbial Biomass Sulphur—An Important Yet Understudied Pool in Soil. Agronomy 11, 1606. doi:
Hu, Z., McKenna, A.M., Wen, K., Zhang, B., Mao, H., Goual, L., Feng, X., Zhu, M., 2024. Controls of Mineral Solubility on Adsorption-Induced Molecular Fractionation of Dissolved Organic Matter Revealed by 21 T FT-ICR MS. Environmental Science & Technology 58, 2313–2322. doi: 10.1021/acs.est.3c08123.
Koch, B.P., Dittmar, T., 2006. From mass to structure: an aromaticity index for high-resolution mass data of natural organic matter. Rapid Communications in Mass Spectrometry 20, 926–932. doi: 10.1002/rcm.2386.
Koch, B.P., Dittmar, T., 2016. Erratum: From mass to structure: an aromaticity index for high-resolution mass data of natural organic matter. Rapid Communications in Mass Spectrometry 30, 250–250. doi: 10.1002/rcm.7433.
Kopittke, P.M., Dalal, R.C., Menzies, N.W., 2016. Sulfur dynamics in sub-tropical soils of Australia as influenced by long-term cultivation. Plant and Soil 402, 211–219. doi: 10.1007/s11104-015-2789-6.
Lavallee, J.M., Soong, J.L., Cotrufo, M.F., 2020. Conceptualizing soil organic matter into particulate and mineral-associated forms to address global change in the 21st century. Global Change Biology 26, 261–273. doi: 10.1111/gcb.14859.
Leuthold, S.J., Haddix, M.L., Lavallee, J., Cotrufo, M.F., 2022. Physical fractionation techniques, Reference Module in Earth Systems and Environmental Sciences. Elsevier, pp. 1–13. doi: https://doi.org/10.1016/B978-0-12-822974-3.00067-7.
Li, X.M., Sun, G.X., Chen, S.C., Fang, Z., Yuan, H.Y., Shi, Q., Zhu, Y.G., 2018. Molecular Chemodiversity of Dissolved Organic Matter in Paddy Soils. Environmental Science & Technology 52, 963–971. doi: 10.1021/acs.est.7b00377.
Liang, C., Schimel, J.P., Jastrow, J.D., 2017. The importance of anabolism in microbial control over soil carbon storage. Nature Microbiology 2, 17105. doi: 10.1038/nmicrobiol.2017.105.
Lindberg, S.E., Garten, C.T., 1988. Sources of sulphur in forest canopy throughfall. Nature 336, 148–151. doi: 10.1038/336148a0.
Manceau, A., Nagy, K.L., 2012. Quantitative analysis of sulfur functional groups in natural organic matter by XANES spectroscopy. Geochimica et Cosmochimica Acta 99, 206–223. doi: https://doi.org/10.1016/j.gca.2012.09.033.

Mao, H.-R., Cotrufo, M.F., Hart, S.C., Sullivan, B.W., Zhu, X., Zhang, J., Liang, C., Zhu, M., 2024. Dual role of silt and clay in the formation and accrual of stabilized soil organic carbon. Soil Biology and Biochemistry 192, 109390. doi: https://doi.org/10.1016/j.soilbio.2024.109390.

Mao, H.-R., Hart, S.C., Peak, D., McKenna, A.M., Zhu, M., 2025. Microbial transformation and mineral adsorption control chemical evolution of soil organic matter during semi-arid ecosystem development. Geochimica et Cosmochimica Acta doi: https://doi.org/10.1016/j.gca.2025.08.041.

McGill, W.B., Cole, C.V., 1981. Comparative aspects of cycling of organic C, N, S and P through soil organic matter. Geoderma 26, 267–286. doi: https://doi.org/10.1016/0016-7061(81)90024-0.

Newman, G.S., Coble, A.A., Haskins, K.E., Kowler, A.L., Hart, S.C., 2020. The expanding role of deep roots during long-term terrestrial ecosystem development. Journal of Ecology doi: 10.1111/1365-2745.13444.

Newman, G.S., Hart, S.C., 2015. Shifting soil resource limitations and ecosystem retrogression across a three million year semi-arid substrate age gradient. Biogeochemistry 124, 177–186. doi: 10.1007/s10533-015-0090-7.

Poulin, B.A., Ryan, J.N., Nagy, K.L., Stubbins, A., Dittmar, T., Orem, W., Krabbenhoft, D.P., Aiken, G.R., 2017. Spatial Dependence of Reduced Sulfur in Everglades Dissolved Organic Matter Controlled by Sulfate Enrichment. Environmental Science & Technology 51, 3630–3639. doi: 10.1021/acs.est.6b04142.

Prăvălie, R., 2016. Drylands extent and environmental issues. A global approach. Earth-Science Reviews 161, 259–278. doi: https://doi.org/10.1016/j.earscirev.2016.08.003.

Prietzel, J., Thieme, J., Salomé, M., Knicker, H., 2007. Sulfur K-edge XANES spectroscopy reveals differences in sulfur speciation of bulk soils, humic acid, fulvic acid, and particle size separates. Soil Biology and Biochemistry 39, 877–890. doi: https://doi.org/10.1016/j.soilbio.2006.10.007.

Prietzel, J., Wu, Y., Dumig, A., Zhou, J., Klysubun, W., 2013. Soil sulphur speciation in two glacier forefield soil chronosequences assessed by S K-edge XANES spectroscopy. European Journal of Soil Science 64, 260–272. doi: 10.1111/ejss.12032.

Ravel, B., Newville, M., 2005. ATHENA, ARTEMIS, HEPHAESTUS: data analysis for X-ray absorption spectroscopy using IFEFFIT. Journal of Synchrotron Radiation 12, 537–541. doi: 10.1107/S0909049505012719.

Reynolds, R., Belnap, J., Reheis, M., Lamothe, P., Luiszer, F., 2001. Aeolian dust in Colorado Plateau soils: Nutrient inputs and recent change in source. Proceedings of the National Academy of Sciences 98, 7123–7127. doi: 10.1073/pnas.121094298.

Reynolds, R., Neff, J., Reheis, M., Lamothe, P., 2006. Atmospheric dust in modern soil on aeolian sandstone, Colorado Plateau (USA): Variation with landscape position and contribution to potential plant nutrients. Geoderma 130, 108–123. doi: https://doi.org/10.1016/j.geoderma.2005.01.012.

Roth, V.-N., Lange, M., Simon, C., Hertkorn, N., Bucher, S., Goodall, T., Griffiths, R.I., Mellado-Vázquez, P.G., Mommer, L., Oram, N.J., Weigelt, A., Dittmar, T., Gleixner, G., 2019. Persistence of dissolved organic matter explained by molecular changes during its passage through soil. Nature Geoscience 12, 755–761. doi: 10.1038/s41561-019-0417-4.

Santana, M.M., Dias, T., Gonzalez, J.M., Cruz, C., 2021. Transformation of organic and inorganic sulfur– adding perspectives to new players in soil and rhizosphere. Soil Biology and Biochemistry 160, 108306. doi: https://doi.org/10.1016/j.soilbio.2021.108306.

Schlesinger, W.H., Raikes, J.A., Hartley, A.E., Cross, A.F., 1996. On the Spatial Pattern of Soil Nutrients in Desert Ecosystems. Ecology 77, 364–374. doi: https://doi.org/10.2307/2265615.

Schroth, A.W., Bostick, B.C., Graham, M., Kaste, J.M., Mitchell, M.J., Friedland, A.J., 2007. Sulfur species behavior in soil organic matter during decomposition. Journal of Geophysical Research: Biogeosciences 112, G04011. doi: 10.1029/2007jg000538.

Selmants, P.C., Hart, S.C., 2008. Substrate age and tree islands influence carbon and nitrogen dynamics across a retrogressive semiarid chronosequence. Global Biogeochemical Cycles 22, GB1021. doi: 10.1029/2007gb003062.

Solomon, D., Lehmann, J., de Zarruk, K.K., Dathe, J., Kinyangi, J., Liang, B.Q., Machado, S., 2011. Speciation and Long- and Short-term Molecular-level Dynamics of Soil Organic Sulfur Studied by X-ray Absorption Near-Edge Structure Spectroscopy. Journal of Environmental Quality 40, 704–718. doi: 10.2134/jeq2010.0061.

Solomon, D., Lehmann, J., Tekalign, M., Fritzsche, F., Zech, W., 2001. Sulfur fractions in particle-size separates of the sub-humid Ethiopian highlands as influenced by land use changes. Geoderma 102, 41–59. doi: https://doi.org/10.1016/S0016-7061(00)00103-8.

Sullivan, T.J., McDonnell, T., McPherson, G., Mackey, S., Moore, D., 2011. Evaluation of the Sensitivity of Inventory and Monitoring National Parks to Acidification Effects from Atmospheric Sulfur and Nitrogen Deposition, Northern Great Plains Network (NGPN). doi:

Takahashi, Y., Kanai, Y., Kamioka, H., Ohta, A., Maruyama, H., Song, Z., Shimizu, H., 2006. Speciation of Sulfate in Size-Fractionated Aerosol Particles Using Sulfur K-Edge X-ray Absorption Near-Edge Structure. Environmental Science & Technology 40, 5052–5057. doi: 10.1021/es060497y.

Tanikawa, T., Sase, H., Fukushima, S., Ito, Y., Yamashita, M., Yamashita, N., Kamisako, M., Sugiyama, A., Imaya, A., Ishida, T., Takenaka, C., Takahashi, M., 2022. Sulfur accumulation in soil in a forested watershed historically exposed to air pollution in central Japan. Geoderma 407, 115544. doi: https://doi.org/10.1016/j.geoderma.2021.115544.

Tfaily, M.M., Chu, R.K., Tolić, N., Roscioli, K.M., Anderton, C.R., Paša-Tolić, L., Robinson, E.W., Hess, N.J., 2015. Advanced Solvent Based Methods for Molecular Characterization of Soil Organic Matter by High-Resolution Mass Spectrometry. Analytical Chemistry 87, 5206–5215. doi: 10.1021/acs.analchem.5b00116.

Turner, B.L., Condron, L.M., France, C.A.M., Lehmann, J., Solomon, D., Peltzer, D.A., Richardson, S.J., 2016. Sulfur dynamics during long-term ecosystem development. Biogeochemistry 128, 281–305. doi: 10.1007/s10533-016-0208-6.

van Veelen, A., Koebernick, N., Scotson, C.S., McKay-Fletcher, D., Huthwelker, T., Borca, C.N., Mosselmans, J.F.W., Roose, T., 2020. Root-induced soil deformation influences Fe, S and P: rhizosphere chemistry investigated using synchrotron XRF and XANES. New Phytologist 225, 1476–1490. doi: https://doi.org/10.1111/nph.16242.

Wilhelm Scherer, H., 2009. Sulfur in soils. Journal of Plant Nutrition and Soil Science 172, 326–335. doi: https://doi.org/10.1002/jpln.200900037.

Wojdyr, M., 2010. Fityk: a general-purpose peak fitting program. Journal of Applied Crystallography 43, 1126–1128. doi: 10.1107/S0021889810030499.

Xia, K., Weesner, F., Bleam, W.F., Helmke, P.A., Bloom, P.R., Skyllberg, U.L., 1998. XANES Studies of Oxidation States of Sulfur in Aquatic and Soil Humic Substances. Soil Science Society of America Journal 62, 1240–1246. doi: https://doi.org/10.2136/sssaj1998.03615995006200050014x.

Xu, C., Wang, S., Chen, Z., Lv, J., Luo, L., Li, J., Ma, Y., 2016. Sulphur speciation and availability in long-term fertilized soil: evidence from chemical fractionation and S K-edge XANES spectroscopy. European Journal of Soil Science 67, 666–675. doi: 10.1111/ejss.12364.

Zeng, T., Arnold, W.A., Toner, B.M., 2013. Microscale Characterization of Sulfur Speciation in Lake Sediments. Environmental Science & Technology 47, 1287–1296. doi: 10.1021/es303914q.

Zhang, Z., Cotrufo, M.F., Turner, B.L., Mao, H.-R., Liang, C., Shakouri, M., Zhu, M., 2026. Mineral stabilization of soil organic sulfur at the continental scale. EarthArXiv doi: https://doi.org/10.31223/X5G49J.

Zhang, Z., Mao, H.-R., Zhao, Z.-Q., Liu, C.-Q., 2024. Effects of small-scale topography on organic sulfur mineralization of subtropical soils. Chemical Geology 660, 122158. doi: https://doi.org/10.1016/j.chemgeo.2024.122158.

Zhao, F.J., Lehmann, J., Solomon, D., Fox, M.A., McGrath, S.P., 2006. Sulphur speciation and turnover in soils: evidence from sulphur K-edge XANES spectroscopy and isotope dilution studies. Soil Biology and Biochemistry 38, 1000–1007. doi: https://doi.org/10.1016/j.soilbio.2005.08.013.

Zhu, M.-X., Chen, L.-J., Yang, G.-P., Huang, X.-L., Zhao, Y.-D., 2016. Composition of organic sulfur in riverine and marine sediments: Insights from sulfur stable isotopes and XANES spectroscopy. Organic Geochemistry 99, 102–112. doi: https://doi.org/10.1016/j.orggeochem.2016.07.002.

Figures and tables

Table 1. Substrate age, geographic coordinates, elevation, climate, and United States Department of Agriculture (USDA) soil taxonomic classification of each of the four sites of the Substrate Age Gradient of Arizona (SAGA). MAP = mean annual precipitation, MAAT = mean annual air temperature, and PET = potential evapotranspiration. Data from (Selmants and Hart, 2008; Newman et al., 2020).

Site	Substrate age (ky)	Latitude, Longitude	Elevation (m)	MAP (mm)	MAAT (°C)	PET (mm y^{-1})	USDA Soil Classification	pH	Dust contribution (%)
Sunset Crater	1	35.394°N, 111.424°W	1905	328	12	1325	Typic Ustorthent	6.57-7.08	8.9
O'Neill Crater	55	35.246°N, 111.459°W	1941	352	11	1328	Typic Durustand	6.40-6.56	42.5
Red Mountain	750	35.538°N, 111.867°W	2073	325	11	1334	Typic Argiustoll	6.39-6.82	86.1
Cedar Mountain	3,000	35.391°N, 112.141°W	2003	338	11	1324	Typic Haplustalf	6.00-6.38	100

Table 2. Soil and microbial properties of the Substrate Age Gradient of Arizona (SAGA). SOC = soil organic carbon, bulk C/N = carbon to nitrogen of bulk soils, MBC/SOC = the ratio of microbial biomass C to SOC, MNC/SOC = the ratio of microbial necromass C to SOC. Data from (Selmants and Hart, 2008; Gu et al., 2019; Mao et al., 2024).

Substrate Age	Canopy type	SOC (g/kg)	Silt+Clay content (g/kg)	Bulk C/N	MBC/SOC (%)	MNC/SOC (%)
1	Inter-	4.1	30	12.0	0.61	19.18
55	canopy	9.2	441	8.9	0.92	42.87
750		17.1	766	10.8	2.43	47.06
3000		13.0	852	9.1	2.47	58.41
1	Pine	6.6	41	14.9	0.37	12.51
55		10.4	417	9.5	0.69	47.06
750		20.6	802	12.4	2.41	37.64
3000		16.3	838	10.3	2.34	50.49
1	Juniper	8.5	72	17.8	0.21	11.94
55		10.3	477	9.8	0.57	42.33
750		19.8	714	11.7	2.66	41.53
3000		15.2	824	9.9	2.82	47.67

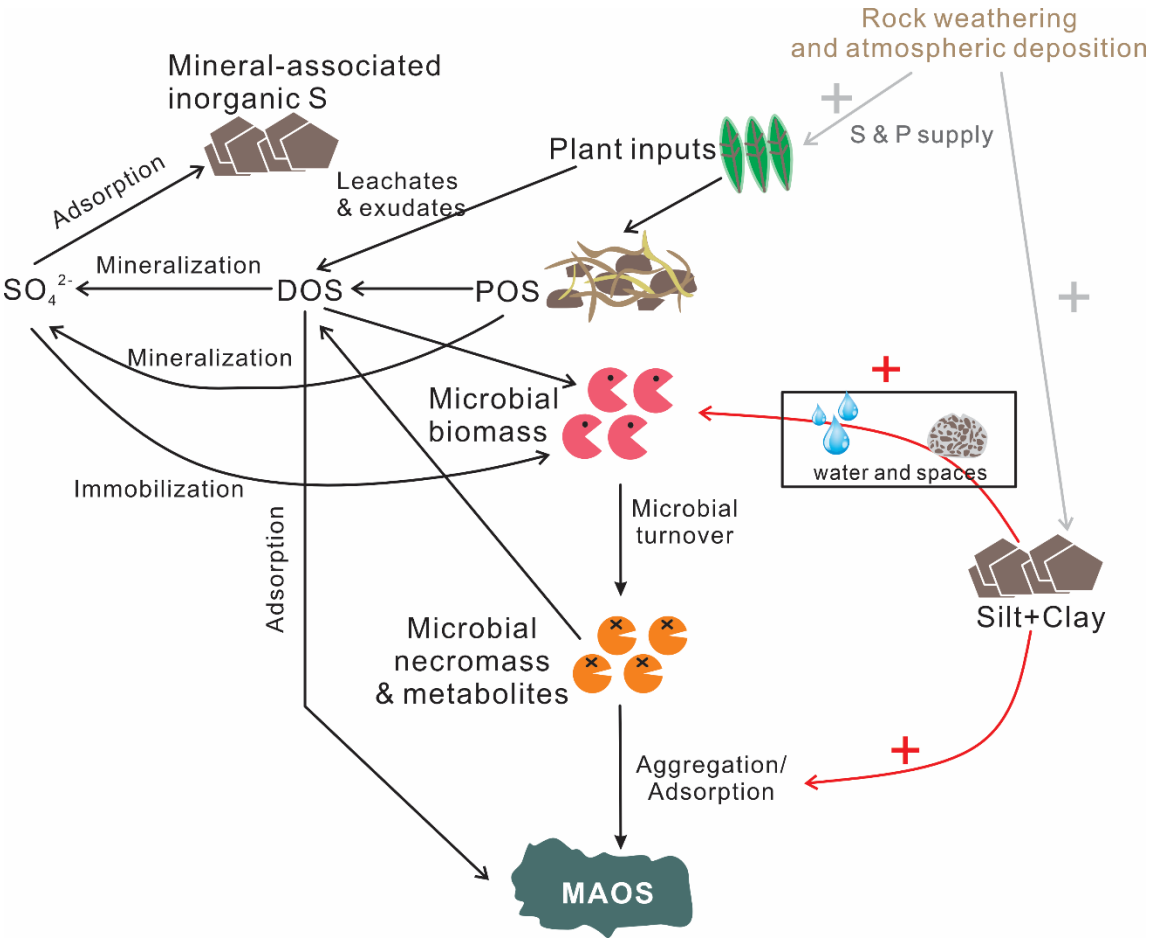

Fig. 1. Conceptual overview of organic sulfur cycling, stabilization, and sulfate availability in developing dryland soils. Plant inputs and microbial turnover transfer S among dissolved organic S (DOS, can be represented by water-extractable organic S), particulate organic S (POS), microbial biomass, and mineral-associated organic S (MAOS). Microbial mineralization releases sulfate, which can be taken up by plants and microbes or retained as exchangeable sulfate on silt- and clay-sized minerals. During soil development, increasing silt and clay contents can enhance microbial activity by improving soil water retention and pore space, while also promoting organic S stabilization through adsorption

and aggregation and retaining released sulfate. This framework illustrates the dual role of fine mineral fractions in regulating organic S persistence and sulfate availability. Arrows indicate major transformation pathways, and red symbols denote mineral effects on microbial and geochemical processes. Other pathways, including desorption, precipitation, and plant uptake, are omitted for clarity.

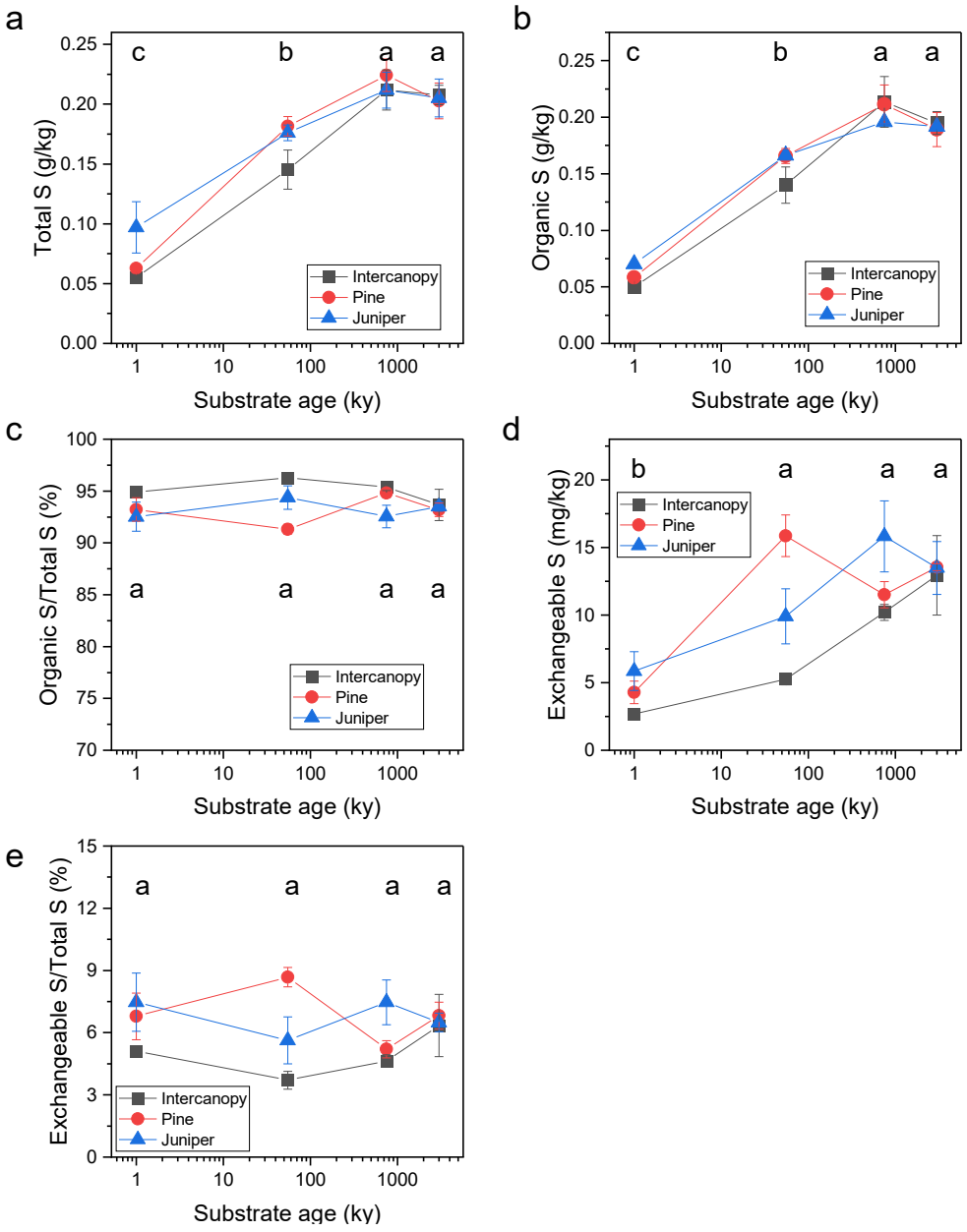

790 **Fig. 2.** Variations in average total sulfur (S) concentration (**a**), organic S concentration (**b**),
791 proportion of organic S to total S (**c**), exchangeable S concentration (**d**), and proportion of
792 exchangeable S to total S (**e**) as a function of substrate age. Error bars represent one
793 standard error. Different letters indicate significant differences across substrate ages for
794 values pooled across canopy types.

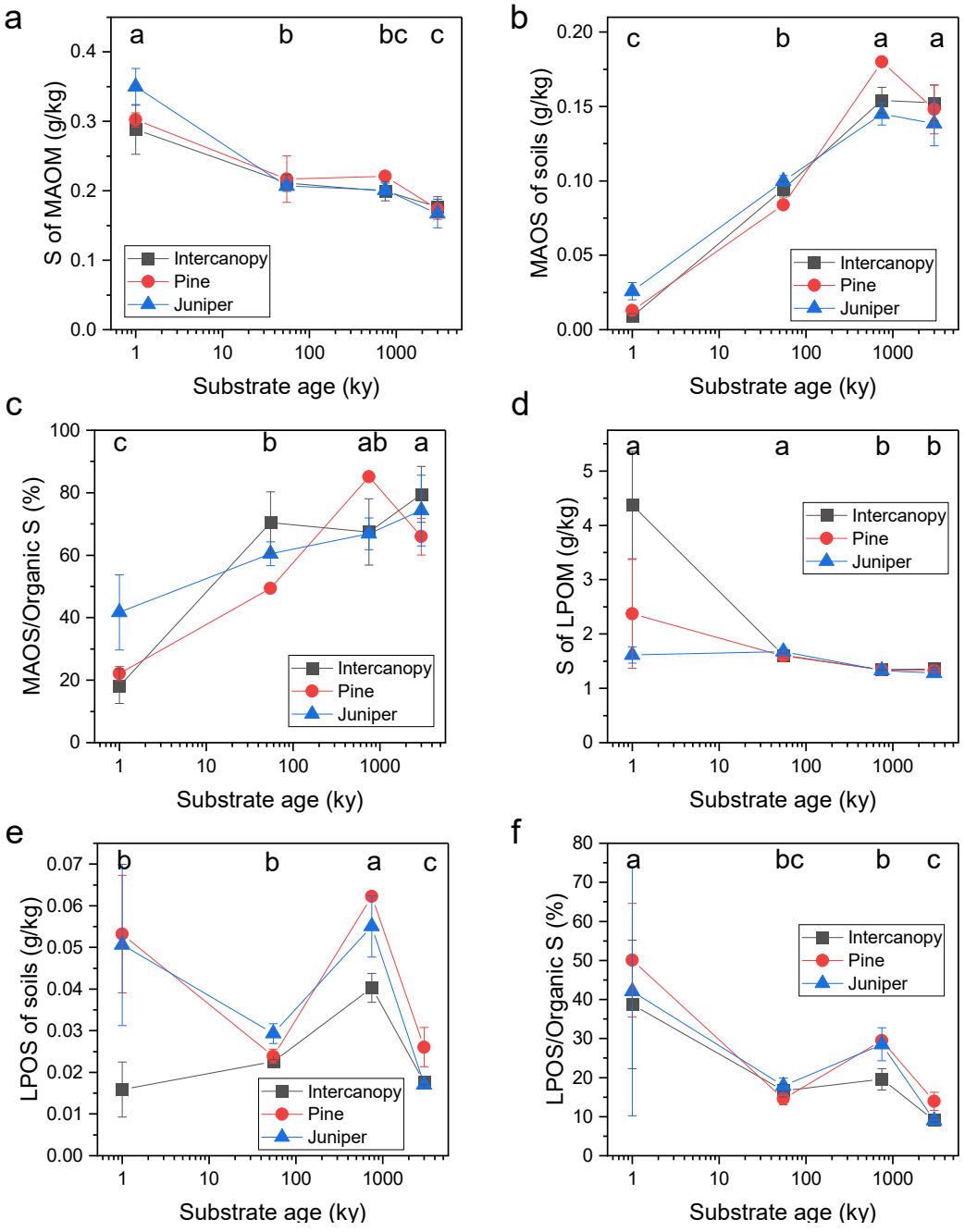

795

Fig. 3. Sulfur (S) in soil organic matter fractions as a function of substrate age. (a) S concentration of mineral-associated organic matter (MAOM), (b) mineral-associated organic S (MAOS) concentration expressed on a bulk-soil basis, (c) proportion of MAOS to total organic S, (d) S concentration of light particulate organic matter (LPOM), (e) light particulate organic S (LPOS) concentration expressed on a bulk-soil basis, and (f) proportion of LPOS to total organic S. Error bars represent one standard error. Different letters indicate significant differences among substrate ages for values pooled across canopy types.

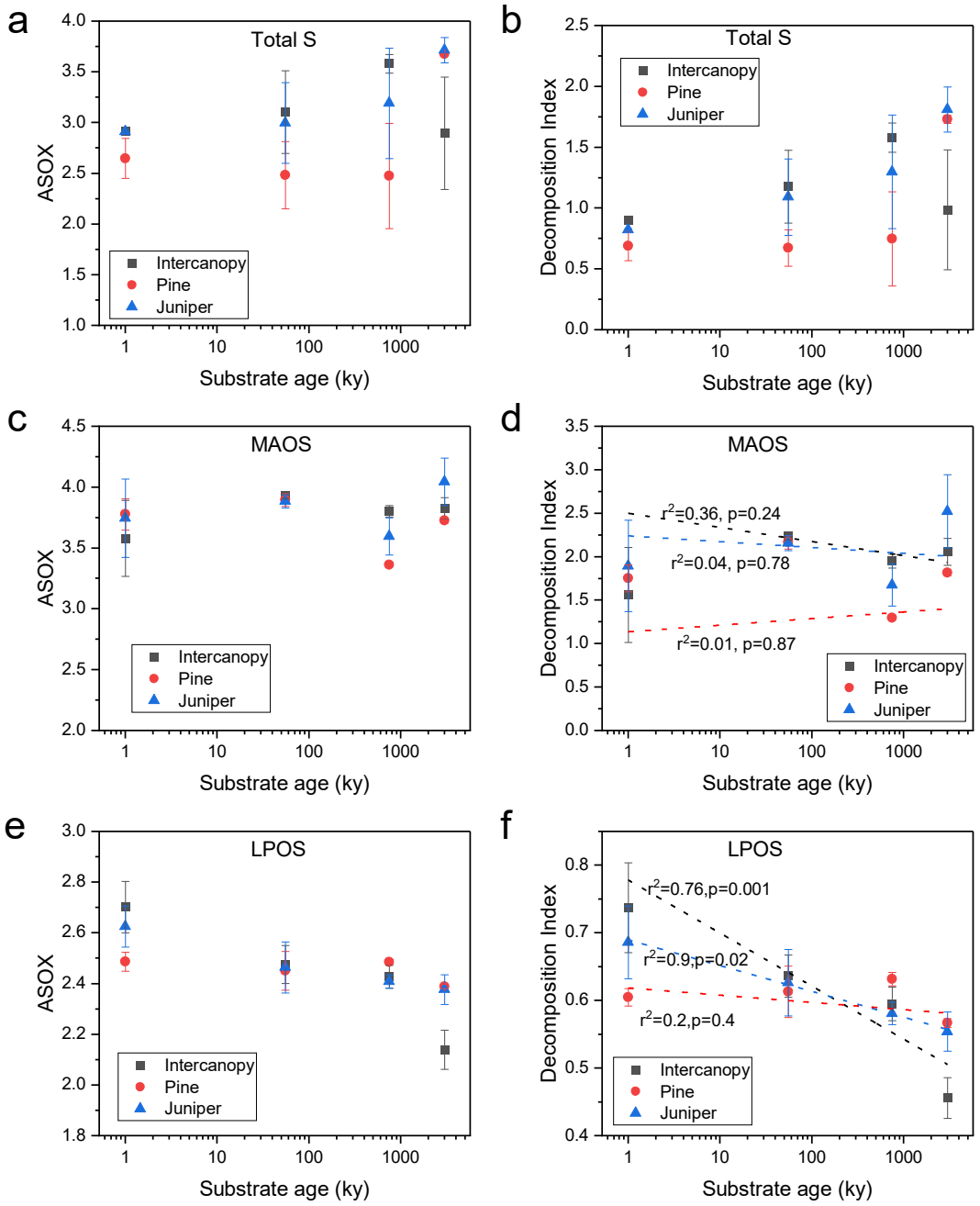

805

806 **Fig. 4.** Variations in average oxidation state (ASOX) and decomposition index of bulk soil

807 organic sulfur (a, b), mineral-associated organic sulfur (c, d), and light particulate organic

808 sulfur (e, f) as a function of substrate age. Error bars represent one standard error.

809

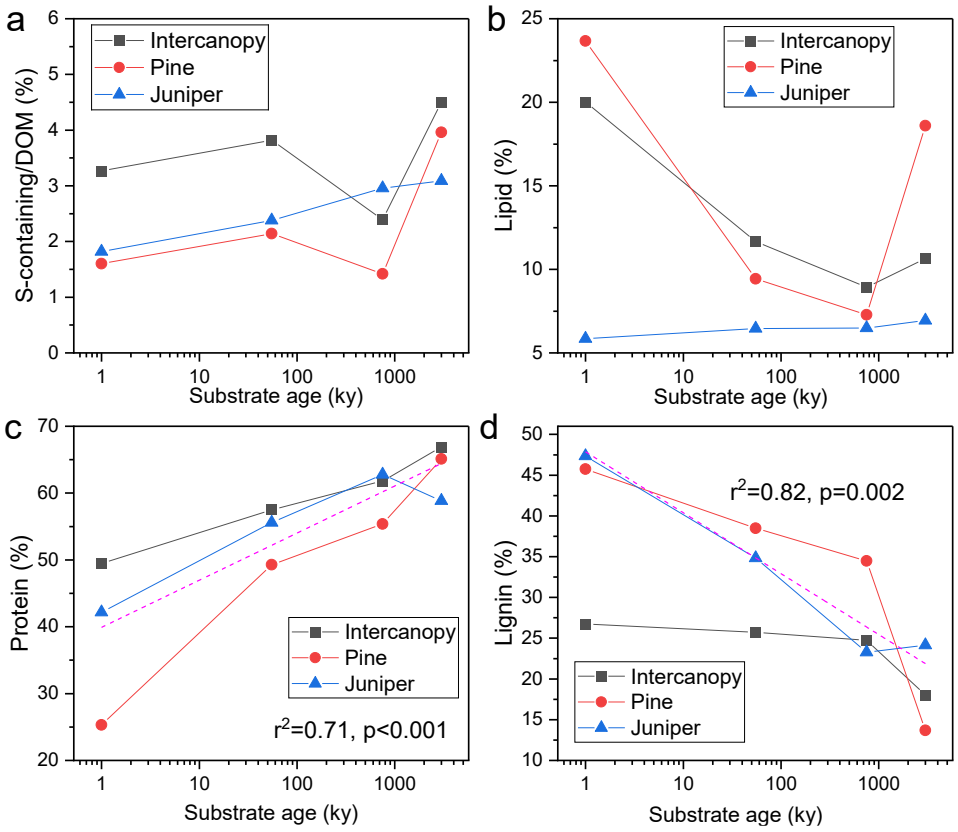

810

811 **Fig. 5**. Proportion of sulfur (S)-containing compounds relative to total dissolved organic

812 matter (DOM) and relative weighted abundance of biochemical classes of water-

813 extractable organic sulfur (WEOS) as a function of substrate age.

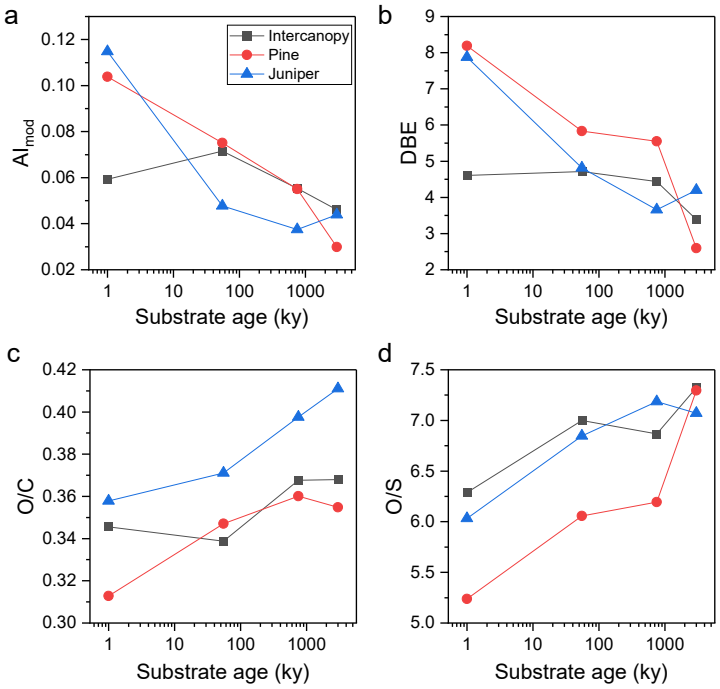

814

815 **Fig. 6.** Molecular parameters of water-extractable organic sulfur as a function of substrate
816 age. Variations in intensity-weighted modified aromaticity index AI_{mod}, double bond
817 equivalence DBE, ratio of oxygen to carbon O/C, and ratio of oxygen to sulfur O/S as a
818 function of substrate age.

819

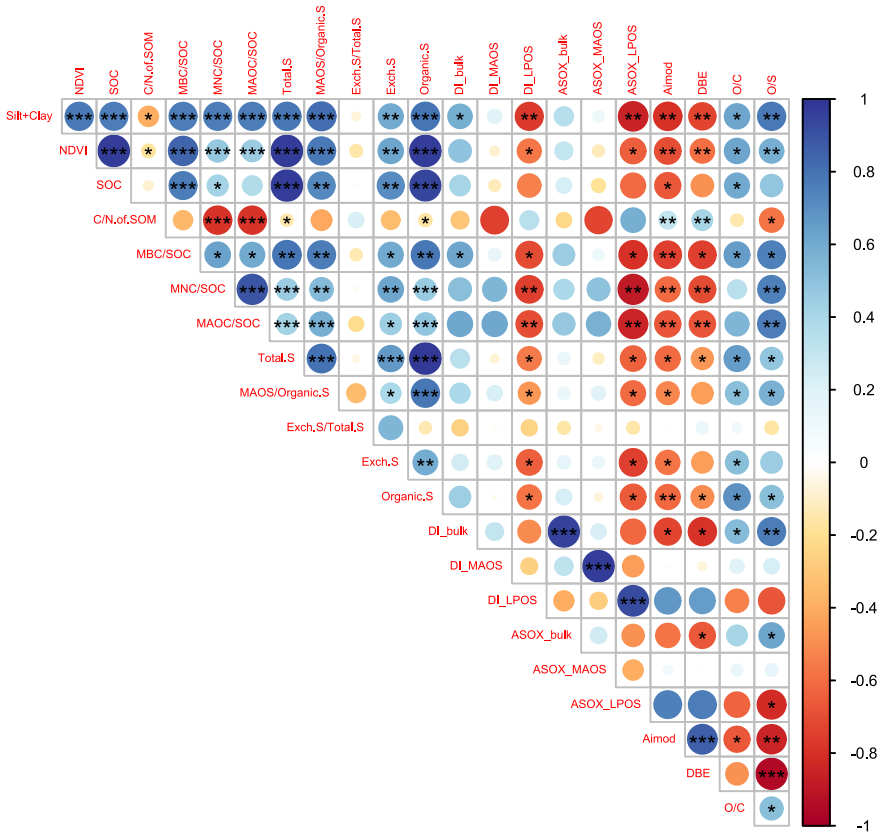

Fig. 7. Correlation heatmap of soil properties and sulfur (S) parameters. The size of the circles indicates the absolute value of the Spearman correlation coefficient. Blue colors indicate positive correlations, and red colors indicate negative correlations. * indicates $p < 0.05$; ** indicates $p < 0.01$; *** indicates $p < 0.001$. Exch.S/total S = exchangeable S to total S; MBC/SOC = microbial biomass C to SOC; MNC/SOC = microbial necromass C to SOC; DI_bulk = decomposition index of bulk soil organic S; DI_MAOS = decomposition index of mineral-associated organic S; DI_LPOS = decomposition index of light particulate organic S; AImod = modified aromaticity index; DBE = double-bond equivalence; O/C = oxygen-to-carbon ratio; O/S = oxygen-to-sulfur ratio.

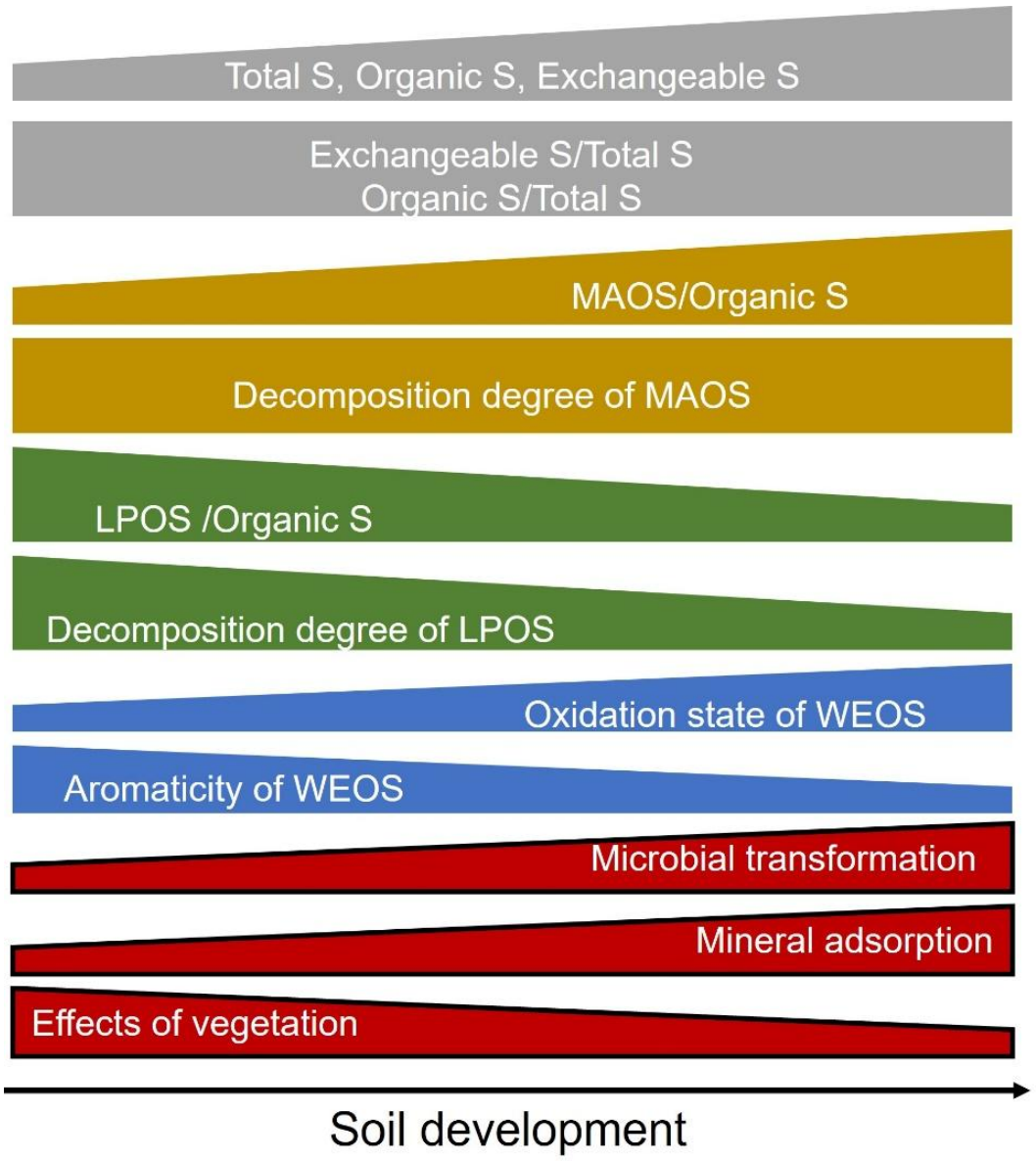

832

833 Fig. 8. Schematic summary of divergent organic sulfur trajectories during dryland soil
834 development. Water-extractable organic sulfur (WEOS) becomes less aromatic, more
835 oxidized, and more microbial-derived; light particulate organic sulfur (LPOS) becomes
836 relatively reduced, consistent with preferential loss of oxidized S species; and mineral-
837 associated organic sulfur (MAOS) remains highly oxidized and decomposed. Together,
838 these patterns support a mineral-filtering model in which fine mineral fractions sort organic
839 S by oxidation state while buffering sulfate availability.